

Showcasing research from Dr Jing Li and Dr Wei Liu's laboratory, Hoffmann Institute of Advanced Materials, Shenzhen Polytechnic, Shenzhen 518055, China.

Crystalline Al_2O_3 modified porous poly(aryl ether ketone) (PAEK) composite separators for high performance lithium-ion batteries via electrospinning technique

A crystalline aluminium oxide (Al_2O_3) nanoparticle coated poly(aryl ether ketone) (PAEK) composite membrane with excellent comprehensive properties was fabricated by an electrospinning technique, and further used as a porous separator for high-performance lithium-ion batteries (LIBs). The cells assembled with the PAEK- Al_2O_3 electrospun non-woven separators exhibited a high initial discharge capacity of more than 158.2 mAh g^{-1} and better cycle retention ratios than the PAEK and commercial PP separators at 0.5 C current density. The obtained PAEK- Al_2O_3 separator exhibited the best effects on the safety and electrochemical properties of the LIBs.

As featured in:





See Wei Liu, Jing Li *et al.*,
CrystEngComm, 2020, **22**, 1577.



Cite this: *CrystEngComm*, 2020, 22, 1577

Crystalline Al₂O₃ modified porous poly(aryl ether ketone) (PAEK) composite separators for high performance lithium-ion batteries via an electrospinning technique†

Hai Li,^a Dawei Luo,^{ab} Jialing He,^d Feng Lin,^b Hao Wang,^a Liang Yu,^a Wei Liu ^{*a} and Jing Li ^{*ca}

The thermostability and wettability of a separator play key roles in improving the safety and electrochemical properties of lithium-ion batteries (LIBs). Given this fact, a crystalline aluminium oxide (Al₂O₃) nanoparticle coated poly(aryl ether ketone) (PAEK) composite membrane with excellent comprehensive properties was fabricated by an electrospinning technique, and further used as a porous separator for high-performance lithium-ion batteries (LIBs). The structure, thermal stability, morphology, liquid electrolyte uptake, porosity, contact angle, ionic conductivity and electrochemical performance of the PAEK–Al₂O₃ blend separator were investigated. Notably, the PAEK–Al₂O₃ separator showed much stronger anti-shrinkage properties (no dimensional changes) than a commercial polypropylene (PP) separator (severe thermal shrinkage) at 150 °C over 1 h. In addition, compared with those of PAEK and commercial PP separators, the degradation temperatures of the PAEK–Al₂O₃ separator were higher, with values over 500 °C. The PAEK–Al₂O₃ separator also had superior electrolyte wettability, and its electrolyte uptake reached 561%. The porosity and ionic conductivity of the composite separator were 89.4% and 3.15 mS cm^{−1}, respectively. As a result of the abovementioned outstanding properties of the blend separator, the cell assembled from the PAEK–Al₂O₃ separator exhibited a high discharge capacity of 158.2 mA h g^{−1} (LiFePO₄/Li⁺) during 100 cycles and a superior C rate performance. Hence, the obtained PAEK–Al₂O₃ separator enhanced the safety and electrochemical properties of the corresponding LIB.

Received 2nd October 2019,
Accepted 14th December 2019

DOI: 10.1039/c9ce01557d

rsc.li/crystengcomm

1. Introduction

Due to high energy density, long cycle life and no memory effect, lithium-ion batteries (LIBs) have been widely applied to portable and dynamic devices such as mobile cellphones and electric vehicles.^{1–3} The separators are sandwiched between the anode and cathode, allowing lithium ions (Li⁺) to transfer quickly during charge–discharge processes and preventing the direct contact of the two electrodes to avoid short-circuits and even explosions.^{4,5} Ideal LIB separators should possess high porosity, better wettability with liquid electrolytes, improved

electrolyte uptake, enhanced thermal and dimensional stability, low electrical resistance, small thickness, and excellent mechanical strength.⁶ Currently, the porous polyolefin separators containing polypropylene (PP), polyethylene (PE) and their derivative composite membranes are often adopted in commercial LIBs on account of their good structure, superior mechanical strength and chemical stability.^{7–10} However, the commercial polyolefin separators still exhibit many disadvantages, for instance, low porosity, poor compatibility with liquid electrolytes and inferior thermal stability.^{11–15} The melting points of PE and PP separators are ~135 °C and ~165 °C, respectively.¹⁶ Celgard company pays attention to the PP/PE/PP trilayer blend separator with a thermal shutdown function. The inferior PE layer will melt and occlude the microvoids at an elevated internal temperature of 130 °C, which prevent further calorification, circuit destruction and even fires.^{17,18} It is a fact that the porous polyolefin separators will suffer from severe thermal shrinkage when the temperature reaches above 90 °C.¹⁹

In order to overcome the shortcomings (especially poor thermal stability) of commercial polyolefin separators and

^a Hoffmann Institute of Advanced Materials, Shenzhen Polytechnic, 7098 Liuxian Blvd, Nanshan District, Shenzhen, 518055, China. E-mail: weiliu2018@szpt.edu.cn

^b School of Applied Chemistry and Biological Technology, Shenzhen Polytechnic, 7098 Liuxian Blvd, Nanshan District, Shenzhen, 518055, China

^c Department of Chemistry and Chemical Biology, Rutgers University, 123 Bevier Road, Piscataway, NJ, 08854, USA. E-mail: jingli@rutgers.edu

^d Library of Shenzhen Polytechnic, Shenzhen Polytechnic, 7098 Liuxian Blvd, Nanshan District, Shenzhen 518055, China

† Electronic supplementary information (ESI) available. See DOI: 10.1039/c9ce01557d

exploit novel high-performance LIB separators, extensive significant studies have been executed in terms of fabrication techniques and developing new-type polymer membranes,²⁰ for instance, stretching techniques, non-solvent induced phase separation, thermally induced phase separation, solvent evaporation-induced phase separation, surface grafting, blending, surface coating, electrospinning techniques and other methods.^{21–25} In order to enhance the thermal stability and affinity with liquid electrolytes, many inorganic nanoparticles (e.g. SiO₂, TiO₂, Al₂O₃, ZrO₂) are used to modify the porous LIB separators.^{26–29} Guoqing Dong *et al.* employed titania (TiO₂) nanoshells to coat a polyimide (PI) nanofiber membrane *via* surface alkaline etching and an *in situ* complexation–hydrolysis strategy, and the composite separator exhibited superior flame-resistance, enhanced thermostability and improved wettability.²¹ Simultaneously, more and more polymers are developed as porous membranes for LIBs, such as poly(acrylonitrile) (PAN), poly(ethylene oxide) (PEO), poly(methyl methacrylate) (PMMA), poly(vinylidene fluoride) (PVDF), polyimide (PI), polyetherimide (PEI) and so on.^{30–35} To some extent, the above-mentioned membranes are easy to swell in polar organic electrolyte liquids and are not adequate to satisfy mechanical strength and thermal stability requirements synchronously.^{8,36}

Poly(aryl ether ketone)s (PAEKs) are a class of functional polymer materials with high thermal stability and enhanced chemical stability.^{37,38} However, PAEK polymers are not readily soluble in various polar organic solvents, which greatly affects their extensive and thorough applications in all respects.¹⁶ Jing Li *et al.* prepared poly(ether ether ketone) (PEEK) with a high ionic conductivity (1.68 mS cm^{−1}) as well as limited solubility by introducing a novel vapor induced demixing method.²¹ In this study, a crystalline Al₂O₃ modified porous PAEK fibrous composite separator (namely PAEK–Al₂O₃) was prepared by an electrospinning technique. The PAEK–Al₂O₃ composite separator combined the respective advantages of crystalline Al₂O₃ nanoparticles and PAEK functional polymer. Therefore, the PAEK–Al₂O₃ blend separator possessed better affinity with organic electrolyte liquids, enhanced thermal stability and improved electrochemical performances compared with commercial polyolefin separators. The electrospun PAEK-based separator has a beneficial affinity for liquid electrolytes that results from its polar structure, which contains fluorinated groups and –O– and –CO– functional groups and exhibits the hydrophilicity of crystalline Al₂O₃ nanoparticles. More notably, the PAEK–Al₂O₃ blend separator has superior thermal stabilities with no thermal shrinkage at 150 °C due to its rigid molecular chain structures and the superior thermostability of the inorganic salts. The cells assembled with the PAEK–Al₂O₃ electrospun non-woven separator exhibited a high initial discharge capacity of more than 158.2 mA h g^{−1}. The electrospun PAEK–Al₂O₃ separator exhibited better cycle retention ratios than the PAEK and commercial PP separators at a high temperature of 25 °C and 0.5 C current density. In short, among the three kinds of separators examined in this study, the obtained PAEK–Al₂O₃ separator

exhibited the best effects on the safety and electrochemical properties of the LIBs.

2. Experimental

2.1. Materials

4,4'-(9H-Fluorene-9,9-diyl)diphenol, bis(4-fluorophenyl)methanone, *N*-methyl-2-pyrrolidone (NMP) and *N,N*-dimethylacetamide (DMAc) were purchased from Shanghai Energy Chemical, Ltd. Potassium carbonate (K₂CO₃), dehydrated toluene, and methanol (Seebio Biomart, Ltd., Shanghai) were used. The cathode, lithium iron phosphate (LiFePO₄), the conductive additive, acetylene black, the binder, polyvinylidene fluoride (PVDF), and the anode, a lithium metal disc, were from Shenzhen Kejing Star Technology Co., Ltd. The organic electrolyte solution composed of 1.0 M LiPF₆ in a liquid mixture of ethyl methyl carbonate (EMC), ethylene carbonate (EC) and dimethyl carbonate (DMC) (with a ratio of 1:1:1, v/v/v) was purchased from Guotai Huarong Company (China). A commercial PP separator (namely, a Celgard 2400 membrane) with 25 μm thickness was employed as a comparative LIB separator. Aluminum foil, hydrochloric acid (HCl), aluminium oxide (Al₂O₃) and other chemicals were used without further handling. The solvents DMAc and NMP were dried using 4 Å molecular sieves prior to use.

2.2. Synthesis of poly(aryl ether ketone) (PAEK)

PAEK was successfully synthesized using the following polymerization procedure: 3 mmol (0.6546 g) of bis(4-fluorophenyl)methanone, 3 mmol (1.0512 g) of 4,4'-(9H-fluorene-9,9-diyl)diphenol, 6 mmol (0.828 g) of K₂CO₃, 10 mL of toluene and 10 mL of DMAc were carefully added into a 50 mL three-neck round-bottom flask equipped with a Dean–Stark trap and a condenser under a nitrogen atmosphere. The mixture was thoroughly stirred into a homogenous solution at room temperature and then heated at 140 °C (oil bath temperature) for 4 h to remove the water. Toluene was used as the azeotropic solvent to remove the water that was formed during the polymerization reaction. Next, the temperature was increased to 175 °C for 5 h to carry out the polymerization and distil the added toluene. Then, the viscous polymer PAEK solution was slowly poured into a beaker containing 100 mL of distilled water and 100 mL of methanol to precipitate the polymer and remove the organic solvent. The polymer precipitate was immersed in a 1 mol L^{−1} HCl solution for 24 h. Finally, the precipitate was pump-filtered and washed with deionized water three times to remove any residual inorganic salts. The fibrous polymer PEEK was dried at 120 °C under vacuum for 24 h (yield: 96%).

2.3. Fabrication of electrospun non-woven fibrous PAEK and PAEK–Al₂O₃ blend separators

A series of fibrous PAEK-based separators including PAEK and PAEK–Al₂O₃ were successfully fabricated into membranes

by an electrospinning technique. A homogenous polymer solution with a weight concentration of 8 wt% was prepared by dissolving the corresponding PAEK polymer in anhydrous NMP and loaded into a 10 mL plastic syringe pump with a stainless steel needle. In addition, 5% by weight crystalline aluminum oxide (Al_2O_3) in the polymer was weighed to prepare an as-mixed solution. During the electrospinning process, the plunger of the syringe containing the corresponding solution was pushed with a flow rate of 0.5 mL h^{-1} , and a high voltage of 20 kV was applied to the metal needle during the whole electrospinning process. The collection distance between the rotating drum wrapped with aluminum foil and the spinneret was 20 cm, and the drum collector was rotated at 200 rpm. The thickness of the electrospun non-woven fibrous separators was approximately controlled to 30 μm . Subsequently, all electrospun PAEK-based non-woven mats were dried in a vacuum oven at 60 $^\circ\text{C}$ for 24 h to remove residual solvent.

2.4. Preparation of electrodes

The cathode electrodes were fabricated in detail as follows: the dried active substance LiFePO_4 , the conductive additive acetylene black and the binder PVDF were mixed together in moderate NMP dispersing agent and stirred for 2 h. The mass ratio of LiFePO_4 , PVDF and acetylene black was 8:1:1. The NMP-based slurry was coated onto flat aluminum current collector foil with a doctor blade. Then, the cathode electrodes were transferred in a vacuum oven at 80 $^\circ\text{C}$ for 12 h to totally evaporate the solvent. The cathode electrodes were further punched into round discs with a diameter of 14 mm, and their active mass loading corresponded to a capacity of approximately 2.0 mA h cm^{-2} . The anode counter electrode was lithium metal. The electrolyte liquid containing 1.0 M LiPF_6 in a mixture of EC, EMC and DMC (1:1:1, v/v/v) was purchased from Guotai Huarong Company (China) and used as received. A CR2032-type coin cell was assembled by sandwiching the electrospun PAEK and PAEK- Al_2O_3 separators and commercial PP separator injected with the organic liquid electrolyte between the LiFePO_4 cathode electrode and lithium metal anode. The conventional commercial PP separator (Celgard 2400) was also injected with the same amount of electrolyte and incorporated in a LIB for comparison. All the above cells were assembled in a dry argon-filled glove box.

2.5. Physical and electrochemical characterization

The chemical structures of the electrospun PAEK and PAEK- Al_2O_3 composite separators were investigated by Fourier transform infrared (FT-IR) spectroscopy using a Nicolet 6700 spectrometer with a wavenumber range of 4000–400 cm^{-1} .

The surface and cross-sectional morphologies of the LIB separators were observed by scanning electron microscopy (SEM, SU-70, Hitachi). The samples for cross-sectional morphology analysis were fractured with liquid nitrogen. To enhance the surface conductivity of the samples for better

quality and resolution of the SEM images, all separators were sputtered with a platinum ion beam for 60 s before taking images.

The porosity (P) of the resultant LIB separators was determined by immersing them in *n*-butanol for 1 h at room temperature and performing the following calculation:

$$P(\%) = \frac{(m_{\text{wet}} - m_{\text{dry}})/\rho}{s \times d} \times 100\% \quad (1)$$

where P is the porosity of the separator, m_{wet} and m_{dry} are the weights of the wet separator and the dry separator, respectively, ρ is the density of the *n*-butanol solvent, and s and d are respectively the area and the thickness of the separator. All measured separators with a thickness of 25 μm were cut into a rectangular shape with a length of 2 cm and a width of 1 cm.

The electrolyte wettability of the separators was measured by an electrolyte droplet method in a glove box filled with argon. All dry separators were cut into round discs with a diameter of 16 mm, and then, 40 μL liquid electrolyte was dropped on the surface of the separators with a pipette.

The electrolyte uptake (EU) of LIB separators was closely connected with Li ion conductivity, defined as the amount of electrolyte absorbed by the membrane, and was calculated from the following equation:

$$\text{EU}(\%) = \frac{W_{\text{wet}} - W_{\text{dry}}}{W_{\text{dry}}} \times 100\% \quad (2)$$

where EU (%) is the electrolyte uptake ratio and W_{dry} and W_{wet} is the weight before and after soaking in electrolyte liquid for 2 h, respectively. Similarly, all separators with an appropriate thickness of 25 μm were cut into a rectangular shape with a length of 2 cm and a width of 1 cm.

The thermal shrinkage of the separators was examined after each sample was deposited at 150 $^\circ\text{C}$ for 1 h. All separators were cut into circles with a 16 mm diameter, and the dimensional changes were photographed during the heat treatment.

In addition, the decomposition temperature and weight change of the LIB separators were determined using a Q50 thermogravimetric (TG) analyzer under a nitrogen flow of 40 mL min^{-1} from 50 $^\circ\text{C}$ to 700 $^\circ\text{C}$ at a heating rate of 10 $^\circ\text{C min}^{-1}$.

The bulk impedance (R_b) of the LIB separators was measured by electrochemical impedance spectroscopy (EIS) using an electrochemical working station CHI660E (Chenhua, China). The experiments were conducted in block-type cells, where the electrolyte-soaked membrane was sandwiched between two stainless-steel (SS) electrodes. Impedance data were recorded in a frequency range from 1 Hz to 10^5 Hz with an AC amplitude of 10 mV under open-circuit potential conditions. The ionic conductivity was obtained according to the following equation:

$$\sigma = \frac{d}{R_b \times S} \quad (3)$$

where σ represents the ionic conductivity and R_b (Ω) is the bulk resistance. In this equation, d is the thickness of the separators and S is recorded as the area of stainless steel. The area of the LIB separator was required to be larger than that of the stainless steel electrode.

The LIB performances, including the charge-discharge behavior, rate capacity and cycle life, were measured using a CR2032 coin half-cell which sandwiched the electrolyte-soaked membrane between LiFePO_4 as the cathode and metallic lithium foil as the anode. The galvanostatic charge-discharge processes of the assembled coin cells were investigated at a current density of 0.5 C within the voltage range of 2.7–4.2 V versus Li/Li^+ by using a CT2001A cell test instrument (LAND Electronic Co., Ltd., China). All tested half-cells were assembled in a dry argon-filled glove box.

3. Results and discussion

3.1. Structures of PAEK

The PAEK polymer was synthesized by one-pot solution polycondensation at a high temperature of 175 °C in DMAc dispersing solvent, as shown in Scheme 1. To obtain a high molecular weight, the solution was very viscous without any precipitates during the experiment.

Fig. 1 shows the Fourier transform infrared (FTIR) spectrum of the PAEK-based separators that were obtained from the above polymeric reaction and electrospinning method. The characteristic stretching vibration peak of the benzene ring was observed at 1592 cm^{-1} . The characteristic absorption peak of carbonyl ($-\text{CO}-$) groups was observed in the spectra at 1655 cm^{-1} . The in-plane bending vibration of C–H was found at 1497 cm^{-1} . The peaks at 1239 cm^{-1} and 1160 cm^{-1} , which corresponded to the asymmetric and symmetric stretching vibrations of C–O–C bonds, indicated the successful synthesis of PAEK. Besides, the additional Al_2O_3 stretching vibrations were found for PAEK- Al_2O_3 at 3062 cm^{-1} and 1447 cm^{-1} . From the results of the FTIR spectral characterization, we confirmed that the corresponding polymers were successfully synthesized.

3.2. Morphology, porosity, EU, and electrolyte wettability of the LIB separators

Fig. 2 shows the pore structures and morphologies of the electrospun PAEK and PAEK- Al_2O_3 LIB separators and the commercial PP separator, which were observed by scanning

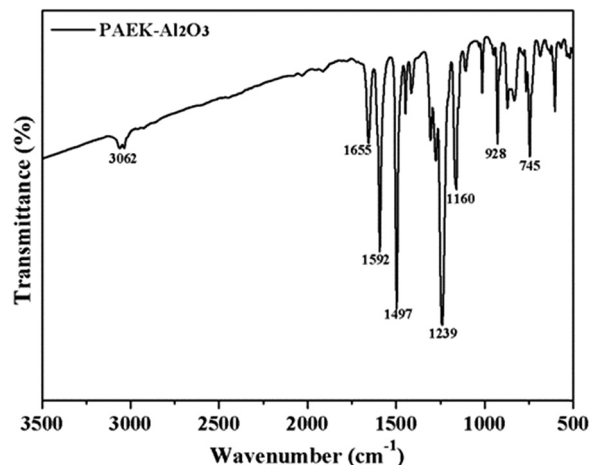


Fig. 1 FTIR spectra of the PAEK- Al_2O_3 separators.

electron microscopy (SEM). Fig. 2(a) shows the surface morphology of the commercial microporous PP membrane, which showed a smooth surface and many elliptical pores with pore diameters in the range of 20–200 nm. Fig. 2(b) shows the cross-sectional morphology of the PP separator, which exhibited peaks and valleys due to the application of a uniaxial stretching technology. Images (c) and (e) display the surface morphologies of the electrospun PAEK and PAEK- Al_2O_3 separators, respectively. The images show that these ether-based LIB separators are composed of countless randomly oriented fibers with fiber diameters ranging from hundreds of nanometers to several micrometers. The intersection of fibers formed interwoven nanopores and increased the mechanical strength of the separators, which was necessary for satisfying the requirements of LIBs. These

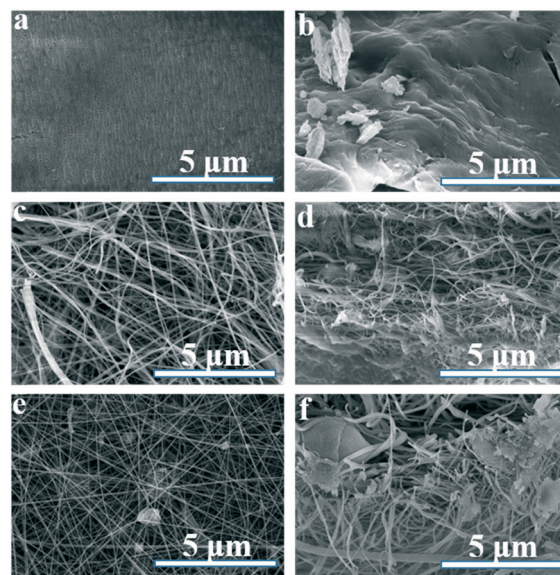
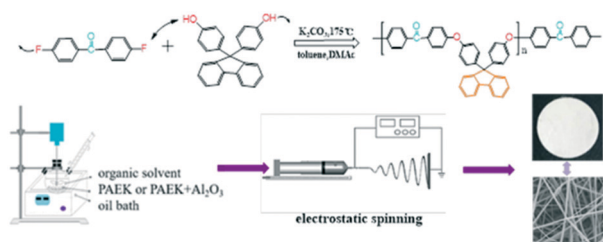


Fig. 2 SEM images of the surface morphologies of the PP (a), PAEK (c), and PAEK- Al_2O_3 (e) separators and the cross-sectional morphologies of the PP (b), PAEK (d), and PAEK- Al_2O_3 (f) separators.



Scheme 1 Schematic of the preparation process for PAEK.

twisted nanopores greatly improved the porosity and specific surfaces, had strong effects on preventing self-discharge and avoiding the internal short circuiting caused by particle migration between the anode and the cathode or dendrite growth, thus enhancing the safety of LIBs.¹² As the microstructural images show, the PAEK polymers were accessibly employed in the electrospinning technique, and as a result, no beads or agglomerates attached to single nanofibers due to the excellent solubility that originated from the abundance of polar functional groups. Besides, the surface morphology of PAEK- Al_2O_3 was characterized by attached flaky crystalline Al_2O_3 which played an important role in entangling the fibers. The nanofibers were clearly cut, and the diameters of the cut fibers were consistent with the diameters measured from the surface images. In short, the morphological structure of the PAEK-based separators was characterized by a high porosity, which is beneficial for improving the uptake and wettability with liquid electrolytes.

The porosity is a crucial parameter of LIB separators, as it can affect the lithium ion conductivity and electrochemical performance. As long as the necessary mechanical strength is provided, a high porosity is preferred for LIB separators because it can help to maintain a sufficient amount of electrolytes and guarantee fast ion transport between two electrodes. Inversely, a low porosity leads to a high internal resistance. As shown in Table 1, the porosities of the electrospun non-woven fibrous PAEK and PAEK- Al_2O_3 separators were 90.7% and 89.4%, respectively. The electrospun nanofibrous separators possessed lower porosities as the fiber diameter decreased. Generally, the electrospun PAEK-based separators had much higher porosities than the commercial PP separator with a porosity of 40%.

The EUs of the electrospun fibrous separators and the commercial PP separator are shown in Table 1. Generally, a high porosity corresponds to a high EU. The EUs of the PAEK and PAEK- Al_2O_3 separators and the commercial PP separator were 514%, 561% and 60%, respectively. The superior EUs of the electrospun PAEK-based polymer separators could be attributed to the good affinity of the polymers with the electrolyte, the large specific surface area of the pore walls and the fully interconnected porous structure. However, the PAEK separator had the highest porosity but not the largest EU because the excessively large pore size caused slight leakage. Notably, the fluorinated separators had a greater EU due to the presence of hydrophilic Al_2O_3 particles intermixed in the fibrous separator.

To obtain a low internal resistance in a cell, a LIB separator should be easily wetted by the liquid electrolyte so that it can absorb and hold onto a significant amount of

electrolyte. As shown in Fig. 3, the wettability of the electrospun PAEK, PAEK- Al_2O_3 and the commercial PP separators was investigated by quickly dropping 40 μL of electrolyte on the surface of each separator. The PP separator was not totally wetted by the liquid electrolyte and generated a liquid droplet due to its poor ability to hold organic solvents and the hydrophobicity of its non-polar structure. In contrast, the surfaces of all the electrospun fibrous membranes were quickly and completely wetted by the electrolyte, which is attributed to the interconnected three-dimensional and highly porous network structures of these membranes with ample polar functional groups. This property was beneficial for transporting lithium ions between the electrodes through the LIB separator. Better lithium ion transport can enhance the comprehensive electrochemical performance of the cells.

3.3. Thermal properties of the LIB separators

Regarding the safety of LIBs, another important property was the thermal dimensional stability of the separators. The separators should maintain dimensional stability at abnormally elevated temperatures to prevent thermal runaway between electrodes and avoid internal/external short circuiting, expansion and even explosion. In the thermal shrinkage measurements of the series of electrospun PAEK-based separators and the commercial PP separator, the dimensional changes were investigated at 150 $^{\circ}\text{C}$ over 1 h. Photographs of the PAEK, PAEK- Al_2O_3 , and PP separators before and after the heat treatment are shown in Fig. 4. The commercial PP separator showed extensive thermal shrinkage due to its intrinsically poor thermal stability with a melting point of approximately 165 $^{\circ}\text{C}$, which also easily caused a color change from white to semi-transparent upon exposure to temperatures above 150 $^{\circ}\text{C}$. Thus, LIBs assembled with the commercial PP separator may suffer from direct contact between the two electrodes at high temperatures. In stark contrast to the low thermal stability of the PP separator, all the electrospun fibrous PAEK-based separators exhibited negligible thermal shrinkage and color changes because of

Table 1 Porosity (*P*), electrolyte uptake (EU) and ionic conductivity (σ) of the obtained electrospun PAEK and commercial PP separators

	PP	PAEK	PAEK- Al_2O_3
<i>P</i> (%)	40	90.7	89.4
EU (%)	60	514	561
σ (mS cm^{-1})	0.66	2.73	3.15

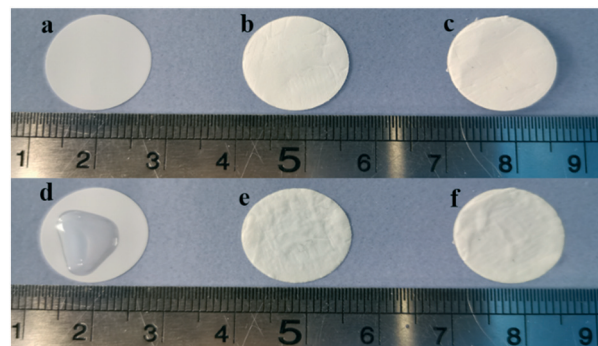


Fig. 3 Wettability images of dry PP (a), PAEK (b) and PAEK- Al_2O_3 (c) separators and wetted PP (d), PAEK (e) and PAEK- Al_2O_3 (f) separators.

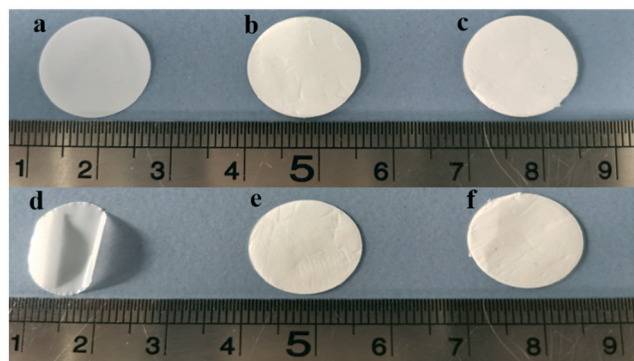


Fig. 4 Thermal shrinkage images of the PP (a), PAEK (b), PAEK- Al_2O_3 (c) separators at 25 °C and PP (d), PAEK (e), PAEK- Al_2O_3 (f) separators at 150 °C for 1 h.

their rigid molecular structures with high intrinsic melting temperatures.

The thermal properties of the LIB separators were further verified by thermogravimetric (TG) analysis. Fig. 5 shows the TG curves of the electrospun porous PAEK and PAEK- Al_2O_3 separators and the commercial PP separator. The thermal degradation of the commercial PP separator was found to start at 350 °C, whereas those of the superior ether-based PAEK polymer separators were not observed until 450 °C. In addition, despite experiencing a high temperature of 700 °C, the PAEK-based separators namely the fibrous PAEK and PAEK- Al_2O_3 separators maintained over 60% residual weight, while the commercial PP separator degraded completely under the same conditions. Compared to the commercial PP separator, all the electrospun fibrous separators show better thermal stabilities, which can be attributed to their rigid aromatic ring molecular chain structure, while PP has a linear polymer structure. The electrospun PAEK- Al_2O_3 composite separator possesses the best thermostability because of the excellent combination of functional PAEK material and heat-resistant inorganic Al_2O_3 nanoparticles.

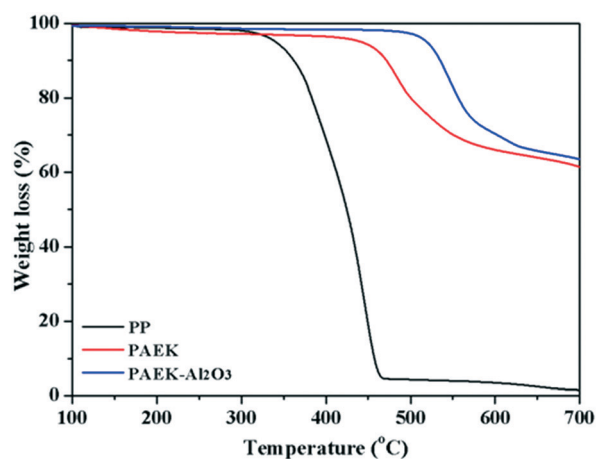


Fig. 5 TGA curves of the electrospun PAEK and PAEK- Al_2O_3 separators and the commercial PP separator.

3.4. Electrochemical properties of the PAEK, PAEK- Al_2O_3 and PP separators

Fig. 6 shows the Nyquist curves of the symmetric cells (*i.e.*, stainless steel/electrolyte-soaked separator/stainless steel) prepared from the electrospun porous PAEK and PAEK- Al_2O_3 separators and the commercial PP separator; the curves were measured by electrochemical impedance spectroscopy (EIS) at 25 °C. The conductivity of the corresponding separator was calculated using the bulk resistance (R_b) of the membrane, which was determined from the intercept of the extrapolated plot at the high-frequency end of the real axis. The electrospun fibrous non-woven PAEK and PAEK- Al_2O_3 composite separators exhibited relatively lower bulk resistances than the commercial PP separator. The bulk resistance of the porous PAEK, PAEK- Al_2O_3 and PP separators was 2.24, 2.02 and 2.91 Ω , respectively. By considering the area of the stainless-steel blocking electrodes and the thickness of the LIB separators, the ionic conductivity was calculated to be 2.73 and 3.15 mS cm^{-1} for PAEK and PAEK- Al_2O_3 , respectively, which were much higher than that of the commercial PP separator with a value of 0.66 mS cm^{-1} , as shown in Table 1. These high ionic conductivities were consistent with the high EUs of the electrospun separators. Ion transport increases with the amount of electrolyte stored in the porous separators, which accordingly enhanced the lithium ion conductivity of an electrolyte-soaked separator. In addition, a higher porosity can provide more channels for lithium ion transport and decrease the resistance. Obviously, the PAEK- Al_2O_3 separator with slightly fluorinated groups had the greatest ionic conductivity due to improved compatibility with the organic liquid electrolyte, which resulted from the comprehensive effects of the EU and porosity; thus, EU may be the main influencing factor. As the fluorine composition increased, the PAEK- Al_2O_3 polymers appeared to swell in the electrolyte to some extent which impaired their corrosion resistance.

The electrochemical stability window is critical for evaluating the electrochemical stability of LIB separators.

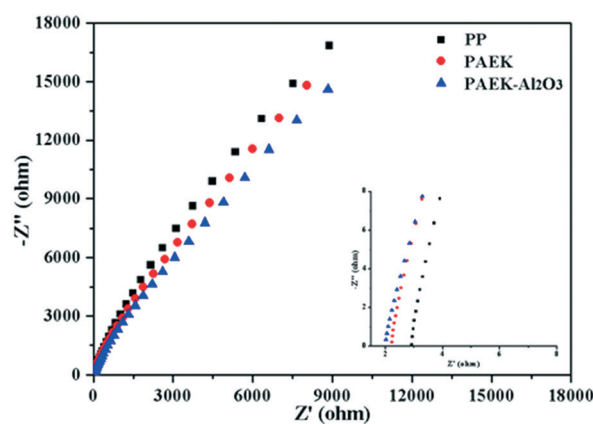


Fig. 6 Nyquist plots of the electrolyte-soaked PAEK, PAEK- Al_2O_3 and commercial PP separators.

Here, the electrochemical stability window is determined by linear sweep voltammetry (LSV) experiments on cell systems (stainless steel|separator|Li) with the electrospun PAEK and PAEK- Al_2O_3 separators and the commercial PP separator. In addition, the LSV experiments were executed with a scan rate of 0.1 mV s^{-1} in the range from 0 to 6 V at room temperature. As shown in Fig. 7, no measurable decomposition of any components in the LIB separators was observed below 4.5 V vs. Li/Li^+ . The electrochemical stability above 5 V may make the electrospun porous fiber separators a promising choice for high-voltage LIB applications.

3.5. Performances of the cells assembled with the PAEK, PAEK- Al_2O_3 and PP separators

To evaluate the long-term stabilities of the separators, the cycle lives of cells assembled with the electrospun porous PAEK and PAEK- Al_2O_3 separators and the commercial PP separator were tested within a voltage range from 2.7 V to 4.2 V with a constant charge current density of 0.5 C at 25 °C. Fig. 8 shows the cycle performance of the cells assembled with the different separators over 100 charge–discharge cycles. Within the first 20 cycles, the discharge capacity of the cell assembled with the commercial PP separator increased from $150.8 \text{ mA h g}^{-1}$ to $152.1 \text{ mA h g}^{-1}$. As more cycles were completed, the PP separator became completely wetted, and the active substance was gradually activated. Then, the discharge capacity became stable and decreased slowly with a final capacity retention of 91.9% after 100 charge and discharge cycles. The LIBs assembled with the electrospun porous PAEK and PAEK- Al_2O_3 separators exhibited larger discharge capacities than the Celgard 2400 membrane, which was attributed to their much higher porosities and better affinities for the liquid electrolyte. The LIBs used with the electrospun separators showed more stable discharge capacities during the 100 cycles and possessed a capacity retention ratio of approximately 94.3% after 100 cycles due to the sufficient wettability of the

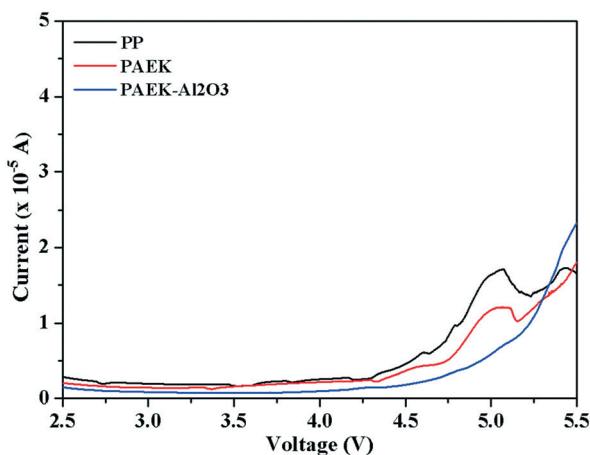


Fig. 7 LSV curves of the cells (stainless steel|separator|Li).

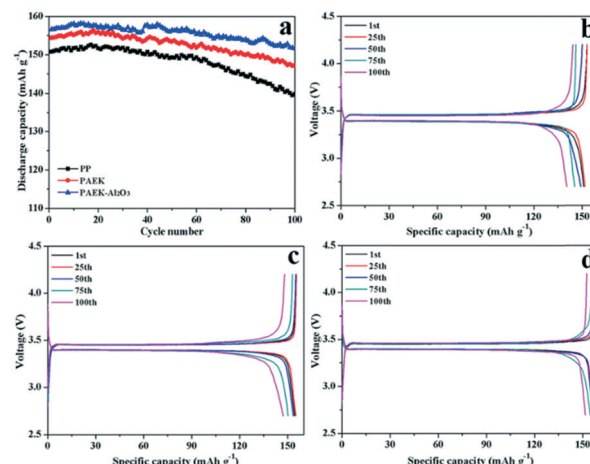


Fig. 8 Discharge cycling performance (a) of the cells at 25 °C and a rate of 0.5 C; charge–discharge curves of the LIBs assembled with the different separators: (b) PP, (c) PAEK and (d) PAEK- Al_2O_3 .

electrospun separators by the electrolyte. The LIB assembled with the electrospun PAEK- Al_2O_3 separator possessed the highest discharge capacity, which corresponded to its best ionic conductivity. The cycle life test implied that the electrospun PAEK- Al_2O_3 separators had adequate chemical and morphological stabilities to function as LIB separators.

The galvanostatic charge and discharge curves of the 1st, 25th, 50th, 75th, and 100th cycles at a constant current of 0.5 C and room temperature of the coin half-cells assembled with the electrospun PAEK and PAEK- Al_2O_3 separators and the commercial PP separator were recorded, and the results are shown in Fig. 8. The charge/discharge curves for all the cells had stable plateaus and good reproducibility, even after 100 cycles, while the cell that contained the electrospun porous PAEK- Al_2O_3 exhibited the highest capacity due to its high porosity, good compatibility with the electrolyte and highest EU. After sufficient wetting of the LIB separator and activation of the LiFePO_4 cathode, the cell capacity decreased gradually with increasing number of charge–discharge cycles (*i.e.*, 1st, 25th, 50th, 75th, and 100th cycle). The initial discharge capacity was 150.8 , 154.4 and $156.6 \text{ mA h g}^{-1}$ for the commercial PP separator and electrospun porous PAEK and PAEK- Al_2O_3 , respectively. The change in the cell discharge capacity was consistent with the trend in the ionic conductivity of each separator.

To estimate the capacity deterioration of each LIB during reversible charge–discharge at high temperature, a cycling test was also carried out at 60 °C and a 0.5 C rate. Fig. 9(a) shows the discharge capacities of the LIBs containing the electrospun PAEK and PAEK- Al_2O_3 separators and the commercial PP separator as a function of the cycle number. Compared to the cycle life measurements at room temperature, all the LIBs exhibit relatively larger capacity fading at 60 °C. After 100 repeated charge–discharge cycles at high temperature, the discharge capacity retention ratio of the cells assembled with the electrospun fibrous PAEK and PAEK- Al_2O_3 separators was 92.8% and 94.5%, respectively.

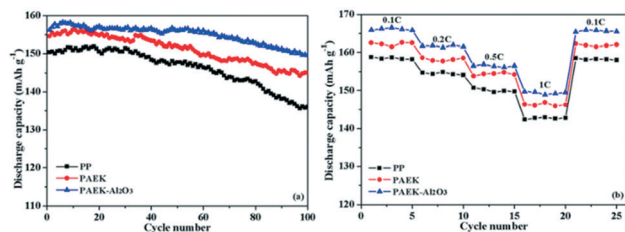


Fig. 9 Discharge cycling performance (a) of the cells at 60 °C and a rate of 0.5 C; rate capabilities (b) of the cells with the electrospun PAEK and PAEK-Al₂O₃ separators and the commercial PP separator.

Furthermore, the discharge capacity of the cell containing the PAEK-Al₂O₃ composite separator decreased from 158.3 mA h g⁻¹ to 149.6 mA h g⁻¹, which is much better than that of the commercial PP separator, whose discharge capacity ranged from 151.9 mA h g⁻¹ to 136 mA h g⁻¹ with an 89.5% retention ratio. These results confirm that the LIBs containing the electrospun porous separators have comparatively better durabilities at high temperature (60 °C) than the LIB made from the commercial PP separator because of their higher ionic conductivity, better compatibility with the liquid electrolyte and greater porosity.

In addition, the rate capacities of coin cells (Li⁺/LiFePO₄) equipped with the electrospun PAEK and PAEK-Al₂O₃ separators and the commercial PP separator were evaluated between 2.7 and 4.2 V at 25 °C, as depicted in Fig. 9(b). The LIBs were discharged continuously with various current densities from 0.1 C to 1 C and back to 0.1 C for 5 cycles each. The cell equipped with the electrospun PAEK-Al₂O₃ composite separator exhibited an excellent capacity retention with increasing C rate and the largest discharge capacity over the various discharge C rates. With the increase in the C rate, a clear distinction between the discharge capacities of the cells was observed at 1 C, where the cell assembled with the PP separator displayed the worst damping. In contrast, the cells containing the electrospun fibrous separators exhibit good electrochemical stabilities and superior rate capacities, which is ascribed to the lower interfacial resistance caused by the better interfacial contact between the electrospun separator and the electrodes and the higher ionic conductivity.

Conclusions

In our work, a series of heat-resistant PAEK-based polymers (including PAEK and PAEK-Al₂O₃) were successfully synthesized by controlling the content of the reactive monomer hexafluorobisphenol A and further fabricated into porous fibrous separators *via* an electrospinning technique. Compared to a commercial PP separator, all the electrospun PAEK-based separators demonstrated much higher porosities and EUs. The ionic conductivities of the fibrous PAEK and PAEK-Al₂O₃ separators and the commercial PP separator were 2.73, 3.15 and 0.66 mS cm⁻¹, respectively, which followed the same trend as the corresponding EUs. More importantly, the cells assembled with the electrospun fibrous separators

exhibited higher discharge capacities and more stable discharge plateaus than that assembled from the commercial PP separator, which was related to the much higher porosity, ionic conductivity and thermal stability of the PAEK-based separators. In particular, the PAEK-Al₂O₃ separator had the best comprehensive performance among the three kinds of LIB separators as a result of its outstanding physical and chemical properties and is a highly competitive separator for application in LIBs.

Conflicts of interest

There are no conflicts to declare.

Acknowledgements

We gratefully acknowledge financial support from the National Natural Science Foundation of China (21901167), the Natural Science Foundation of Guangdong Province (2018A030313371), and the Shenzhen Sci and Tech Innovation Commission (JCYJ20180307102051326).

Notes and references

- 1 C. Xi, Q. Chengjun, D. Wei, L. Jingwen, M. Xiaoming, Z. Yulu, L. Tao, T. Xiaoma, C. Hongmei and O. Yifang, *J. Phys. D: Appl. Phys.*, 2018, **51**, 405103.
- 2 H. Zhao, N. Deng, J. Ju, Z. Li, W. Kang and B. Cheng, *Mater. Lett.*, 2019, **236**, 101–105.
- 3 J. Zhao, Q. Hu, J. Wang, P. Zhang, Y. Zhu, G. Wu, Y. Lv, L. Lv, Y. Zhao and M. Yang, *Coatings*, 2018, **8**, 437.
- 4 W. Xie, W. Liu, Y. Dang, A. Tang, T. Deng and W. Qiu, *J. Power Sources*, 2019, **417**, 150–158.
- 5 G. Zeng, J. Zhao, C. Feng, D. Chen, Y. Meng, B. Boateng, N. Lu and W. He, *ACS Appl. Mater. Interfaces*, 2019, **11**, 26402–26411.
- 6 X. Yang, X. Zhang, J. Deng, Z. Chu, Q. Jiang, J. Meng, P. Wang, L. Zhang, Z. Yin and J. You, *Nat. Commun.*, 2018, **9**, 570.
- 7 D. Chen, Z. Zhou, C. Feng, W. Lv, Z. Wei, K. H. L. Zhang, B. Lin, S. Wu, T. Lei, X. Guo, G. Zhu, X. Jian, J. Xiong, E. Traversa, S. X. Dou and W. He, *Adv. Energy Mater.*, 2019, **9**, 1803627.
- 8 Z. Qiu, L. Shi, Z. Wang, J. Mindemark, J. Zhu, K. Edström, Y. Zhao and S. Yuan, *Chem. Eng. J.*, 2019, **368**, 321–330.
- 9 M. Waqas, S. Ali, C. Feng, D. Chen, J. Han and W. He, *Small*, 2019, **15**, e1901689.
- 10 N. Wei, J. Hu, M. Zhang, J. He and P. Ni, *Electrochim. Acta*, 2019, **307**, 495–502.
- 11 M. Cai, J. Zhu, C. Yang, R. Gao, C. Shi and J. Zhao, *Polymer*, 2019, **11**, 1–11.
- 12 C. Deng, Y. Jiang, Z. Fan, S. Zhao, D. Ouyang, J. Tan, P. Zhang and Y. Ding, *Appl. Surf. Sci.*, 2019, **484**, 446–452.
- 13 W. Xie, W. Liu, Y. Dang and Y. Peng, *Polym. Int.*, 2019, **68**, 1341–1350.
- 14 G. Xu, L. Ding, T. Wu, M. Xiang and F. Yang, *J. Polym. Res.*, 2019, **26**, 1–14.

- 15 H. Xu, M. Li, K. Han, J. Xiao, X. Chen and Y. Li, *IOP Conf. Ser.: Mater. Sci. Eng.*, 2019, **493**, 012080.
- 16 H. Li, B. Zhang, B. Lin, Y. Yang, Y. Zhao and L. Wang, *J. Electrochem. Soc.*, 2018, **165**, A939–A946.
- 17 M. Waqas, S. Ali, W. Lv, D. Chen, B. Boateng and W. He, *Adv. Mater. Interfaces*, 2018, **6**, 1801330.
- 18 F. Zeng, R. Xu, L. Ye, B. Xiong, J. Kang, M. Xiang, L. Li, X. Sheng and Z. Hao, *Ind. Eng. Chem. Res.*, 2019, **58**, 2217–2224.
- 19 G. Zhong, Y. Wang, C. Wang, Z. Wang, S. Guo, L. Wang, X. Liang and H. Xiang, *Ionics*, 2018, **25**, 2677–2684.
- 20 X. Tian, B. Xin, Z. Lu, W. Gao and F. Zhang, *RSC Adv.*, 2019, **9**, 11220–11229.
- 21 G. Dong, B. Liu, G. Sun, G. Tian, S. Qi and D. Wu, *J. Membr. Sci.*, 2019, **577**, 249–257.
- 22 J. Y. Kim, D. O. Shin, K. M. Kim, J. Oh, J. Kim, S. H. Kang, M. J. Lee and Y. G. Lee, *Sci. Rep.*, 2019, **9**, 2464.
- 23 J. Li, X. Niu, J. Song, Y. Li, X. Li, W. Hao, J. Fang and T. He, *J. Membr. Sci.*, 2019, **577**, 1–11.
- 24 J. Liu, X. Shi, B. Boateng, Y. Han, D. Chen and W. He, *ChemSusChem*, 2019, **12**, 908–914.
- 25 L. Wang, Z. Wang, Y. Sun, X. Liang and H. Xiang, *J. Membr. Sci.*, 2019, **572**, 512–519.
- 26 D. Li, D. Shi, Z. Yuan, K. Feng, H. Zhang and X. Li, *J. Membr. Sci.*, 2017, **542**, 1–7.
- 27 C. Shi, J. Dai, X. Shen, L. Peng, C. Li, X. Wang, P. Zhang and J. Zhao, *J. Membr. Sci.*, 2016, **517**, 91–99.
- 28 J.-H. Yoo, W.-K. Shin, S. M. Koo and D.-W. Kim, *J. Power Sources*, 2015, **295**, 149–155.
- 29 L. Zhang, G. Feng, X. Li, S. Cui, S. Ying, X. Feng, L. Mi and W. Chen, *J. Membr. Sci.*, 2019, **577**, 137–144.
- 30 S. Byun, S. H. Lee, D. Song, M.-H. Ryou, Y. M. Lee and W. H. Park, *J. Ind. Eng. Chem.*, 2019, **72**, 390–399.
- 31 W. Gong, S. Wei, S. Ruan and C. Shen, *Mater. Lett.*, 2019, **244**, 126–129.
- 32 S. Wang, D. Zhang, Z. Shao and S. Liu, *Carbohydr. Polym.*, 2019, **214**, 328–336.
- 33 Q.-Y. Wu, H.-Q. Liang, L. Gu, Y. Yu, Y.-Q. Huang and Z.-K. Xu, *Polymer*, 2016, **107**, 54–60.
- 34 H. Xu, D. Li, Y. Liu, Y. Jiang, F. Li and B. Xue, *J. Alloys Compd.*, 2019, **790**, 305–315.
- 35 X. Zhang, N. Li, Z. Hu, J. Yu, Y. Wang and J. Zhu, *J. Membr. Sci.*, 2019, **581**, 355–361.
- 36 H. Zheng, Z. Wang, L. Shi, Y. Zhao and S. Yuan, *J. Colloid Interface Sci.*, 2019, **554**, 29–38.
- 37 A. Le Mong and D. Kim, *J. Power Sources*, 2016, **304**, 301–310.
- 38 D. Li, D. Shi, K. Feng, X. Li and H. Zhang, *J. Membr. Sci.*, 2017, **530**, 125–131.